

1. Extended Data

Figure #	Figure title One sentence only	Filename This should be the name the file is saved as when it is uploaded to our system. Please include the file extension. i.e.: <i>Smith_ED_Fi_1.jpg</i>	Figure Legend If you are citing a reference for the first time in these legends, please include all new references in the Online Methods References section, and carry on the numbering from the main References section of the paper.
Extended Data Fig. 1			
Extended Data Fig. 2			
Extended Data Fig. 3			
Extended Data Fig. 4			
Extended Data Fig. 5			
Extended Data Fig. 6			
Extended Data Fig. 7			
Extended Data Fig. 8			
Extended Data Fig. 9			
Extended Data Fig. 10			

2. Supplementary Information:

A. Flat Files

Item	Present?	Filename This should be the name the file is saved as when it is	A brief, numerical description of file contents. i.e.: <i>Supplementary Figures 1-4, Supplementary Discussion, and</i>	
------	----------	---	---	--

		uploaded to our system, and should include the file extension. The extension must be .pdf	Supplementary Tables 1-4.	
Supplementary Information	Yes	McKenna_et_al_supplementary_information.pdf	Supplementary Figures 1-8, Supplementary Tables 1-3	
Reporting Summary	No			

B. Additional Supplementary Files

Type	Number If there are multiple files of the same type this should be the numerical indicator. i.e. "1" for Video 1, "2" for Video 2, etc.	Filename This should be the name the file is saved as when it is uploaded to our system, and should include the file extension. i.e.: <i>Smith_Supplementary_Video_1.mov</i>	Legend or Descriptive Caption Describe the contents of the file
Choose an item.			
Choose an item.			
Choose an item.			
Choose an item.			
Choose an item.			
Choose an item.			

3. Source Data

Parent Figure or Table	Filename This should be the name the file is saved as when it is uploaded to our system, and should include the file extension. i.e.: <i>Smith_SourceData_Fig1.xls</i> , or <i>Smith_Unmodified_Gels_Fig1.pdf</i>	Data description e.g.: Unprocessed Western Blots and/or gels, Statistical Source Data, etc.
Source Data Fig. 1		
Source Data		

Fig. 2		
Source Data Fig. 3		
Source Data Fig. 4		
Source Data Fig. 5		
Source Data Fig. 6		
Source Data Fig. 7		
Source Data Fig. 8		
Source Data Extended Data Fig. 1		
Source Data Extended Data Fig. 2		
Source Data Extended Data Fig. 3		
Source Data Extended Data Fig. 4		
Source Data Extended Data Fig. 5		
Source Data Extended Data Fig. 6		
Source Data Extended Data Fig. 7		
Source Data Extended Data Fig. 8		
Source Data Extended Data Fig. 9		
Source Data Extended Data Fig. 10		

Stringent mitigation substantially reduces risk of unprecedented near-term warming rates

Christine M. McKenna^{1,*}, Amanda C. Maycock¹, Piers M. Forster¹,
Christopher J. Smith^{1,2}, and Katarzyna B. Tokarska³

¹ School of Earth and Environment, University of Leeds, Leeds, UK

² International Institute for Applied Systems Analysis (IIASA), Laxenburg, Austria

³ Institute for Atmospheric and Climate Science, ETH Zurich, Zurich, Switzerland

* Corresponding author: C.McKenna1@leeds.ac.uk

14 **Abstract**

15 Following the Paris Agreement, many countries are enacting targets to achieve net-zero
16 greenhouse gas emissions. Stringent mitigation will have clear societal benefits in the second
17 half of this century by limiting peak warming and stabilizing climate. However, the near-term
18 benefits of mitigation are generally thought to be less clear because forced surface temperature
19 trends can be masked by internal variability. Here we use observationally-constrained
20 projections from the latest comprehensive climate models and a simple climate model emulator,
21 to show that pursuing stringent mitigation consistent with holding long-term warming below 1.5
22 °C reduces the risk of unprecedented warming rates in the next 20 years by a factor of 13
23 compared to a no-mitigation scenario, even after accounting for internal variability. Therefore, in
24 addition to long-term benefits, stringent mitigation offers substantial near-term benefits by
25 offering societies and ecosystems a greater chance to adapt to and avoid the worst climate
26 change impacts.

Main text

Near-term warming rates affect how rapidly society and ecosystems must adapt to the worst impacts of climate change. Recent decades have seen high rates of global average surface warming; the maximum warming trend for 20-year segments of the observation-based record since pre-industrial times is $0.27\text{ }^{\circ}\text{C decade}^{-1}$, which occurred in the last few decades with the exact timing dependent on the dataset used (Supplementary Fig. 1). It is clear that to stabilize climate in the long-term, global net-zero greenhouse gas emissions must be achieved¹; however, it is less clear when the benefits of mitigation applied now will become evident²⁻⁶.

Here, we investigate the effect of different levels of mitigation in future emission scenarios on surface warming rates in the next 20 years (2021-2040), a key period for policymakers at the forefront of climate change adaptation. For example, crop breeding is unlikely to keep pace with climate impacts on agriculture over this period under current rates of warming⁷. The next 20 years is also a typical time horizon for initial planning to operation of large-scale structural responses to support climate change adaptation, such as the design and implementation of flood defences⁸.

The general consensus is that differences in global mean surface temperature between high and low emission pathways only emerge after roughly the 2050s, with changes not being detectable beforehand²⁻⁶. The long atmospheric lifetime of CO_2 means that substantial emission reductions are needed to alter the upwards trend in atmospheric concentration and effective radiative forcing⁹, making it difficult for society to notice the immediate benefits of mitigation efforts. While the Paris Agreement long-term targets are concerned with addressing the anthropogenic warming contribution¹⁰⁻¹¹, the temperature changes society will experience in the near-term will come from a combination of a forced response to radiative forcings and internal climate variability¹²⁻¹³. On decadal timescales, internal variability can overwhelm the forced

climate response, even for spatially averaged quantities like global temperature⁴, having profound implications for the public understanding of climate change. For example, the period of relatively slow surface warming between around 1998 and 2012, which was partly associated with internal climate variability¹⁴, was widely misreported leading to doubt in the public mind about how well anthropogenic climate change is understood¹⁵. It is therefore important to communicate to what extent strong mitigation efforts will offer benefits in the near-term as well as in the long-term, and to what extent those benefits may be masked on shorter timescales by internal variability.

Here, we combine two approaches (see Methods) to assess whether mitigation has detectable benefits for near-term warming rates. The first approach uses projections from the latest Coupled Model Intercomparison Project Phase 6 (CMIP6) models, driven by Shared Socioeconomic Pathway (SSP¹⁶) scenarios and constrained according to their representation of recent observed warming rates¹⁷. The second approach uses a simple climate model emulator (FaIR¹⁸), with added observation-based estimates of internal variability¹⁹, also run under SSP scenarios and, additionally, a scenario consistent with current and projected pledges as of 2019 in the Nationally Determined Contributions (NDCs) under the Paris Agreement²⁰⁻²². Simple climate models like FaIR are designed to emulate the behavior of more complex climate models in a computationally inexpensive way, by using simplified representations of the physical relationships between emissions, atmospheric concentrations of greenhouse gases and other climate forcers, radiative forcing, and temperature change. The combination of these two approaches is advantageous because the CMIP6 models - while comprehensive - do not necessarily accurately represent observed internal variability, and CMIP6 was not designed to fully sample the range of parameter uncertainties that affect temperature projections. Since FaIR is inexpensive to run, it can be used to more broadly sample uncertainty in temperature projections than individual complex climate models (see Methods).

We focus on strong mitigation pathways in line with the Paris Agreement 1.5 °C and 2 °C long-term temperature targets (SSP1-1.9 and SSP1-2.6, respectively), and include the NDC-like scenario to consider a less ambitious and more plausible mitigation pathway²³. These are compared to baseline no mitigation pathways (SSP3-7.0 and SSP5-8.5). SSP5-8.5 is a highly unlikely “worst case” no mitigation pathway since, for example, it assumes a fivefold increase in coal use by the late 21st century²³. Conversely, SSP3-7.0 represents an “average” no mitigation pathway²³ and, as such, focus will be placed on this as a baseline.

Firstly, we ask whether over the next 20 years, mitigation – relative to a baseline of no mitigation – will reduce: (i) the risk of experiencing unprecedented warming rates (exceeding the highest warming rate observed to date), and (ii) the potential magnitude of extreme warming rates (i.e., low probability 20-year trends in the upper 5th percentile), which could lead to the failure of adaptation plans.

Both the CMIP6 and FaIR simulations show a clear benefit of strong mitigation in terms of decreasing near-term warming rates (Fig. 1a). The following results are quoted from the FaIR projections accounting for internal variability, but note that the distributions of trends for the constrained CMIP6 models are in good agreement with FaIR (Fig. 1a). In the strong mitigation scenario consistent with warming of below 2.0 °C by 2100 (SSP1-2.6; blue boxes), the median warming rate is almost half that in the “worst case” no mitigation scenario (SSP5-8.5; brown boxes), and two thirds that in the “average” no mitigation scenario (SSP3-7.0; orange boxes).

Under the even stronger mitigation scenario consistent with keeping long-term warming below 1.5 °C (SSP1-1.9; green box), the median warming rate is almost one third of that in the “worst case” no mitigation scenario, and just over half that in the “average” no mitigation scenario.

Even under less ambitious mitigation consistent with current and projected NDCs (grey box), there is still a reduction in median warming rate by around one third compared to SSP5-8.5 and one quarter compared to SSP3-7.0. The median effective radiative forcing (ERF) trend in FaIR

over this period differs by $0.63 \text{ W m}^{-2} \text{ decade}^{-1}$ between SSP1-1.9 and SSP5-8.5 (Supplementary Table 1), which comes mainly from carbon dioxide ($0.42 \text{ W m}^{-2} \text{ decade}^{-1}$), methane ($0.15 \text{ W m}^{-2} \text{ decade}^{-1}$), tropospheric ozone ($0.13 \text{ W m}^{-2} \text{ decade}^{-1}$), and other well-mixed greenhouse gases ($0.05 \text{ W m}^{-2} \text{ decade}^{-1}$), with a slight offset from anthropogenic aerosols ($-0.16 \text{ W m}^{-2} \text{ decade}^{-1}$). The difference in near-term total ERF trend is $0.29 \text{ W m}^{-2} \text{ decade}^{-1}$ between SSP1-2.6 and SSP3-7.0 (Supplementary Table 1). Over the next 20 years, the difference in median ERF trends between the strong mitigation and no mitigation SSP scenarios are therefore comparable to, or larger than, the total ERF trend over the recent past (1995-2014; $0.40 \text{ W m}^{-2} \text{ decade}^{-1}$; Supplementary Table 1).

Comparing the distributions of projected warming rates to the maximum trend for 20-year segments of the observation-based record since the pre-industrial (red ticks on y-axes, Fig. 1a), we find that strong mitigation has a discernible effect on the risk of experiencing stronger warming than observed in the past, even after accounting for internal variability. Under SSP1-1.9 (SSP1-2.6) there is only a 4% (14%) probability of the warming rate in the next 20 years exceeding the maximum observed trend, while for SSP3-7.0 (SSP5-8.5) this increases considerably to a 54% (75%) probability. Less ambitious mitigation, in line with current and projected NDCs, results in a higher probability (21%) of unprecedented near-term warming than for SSP1-1.9 or SSP1-2.6. Pursuing rapid, stringent mitigation therefore substantially reduces the risk of experiencing unprecedented warming rates over the next 20 years, giving society and ecosystems a greater chance to adapt to and avoid the worst impacts of climate change. Indeed, for warming rates of $0.3 \text{ }^{\circ}\text{C decade}^{-1}$, which is close to the threshold for unprecedented warming rates, it has been estimated only 30% of all climate change impacted ecosystems can adapt and only 17% of impacted forests²⁴.

Note that very high near-term warming rates, which are substantially larger than the maximum observed historical 20-year trend, are still possible in all scenarios considered. However, a key

point for policymakers to note is that strong mitigation greatly reduces the extremity of these low probability high impact cases, reducing the risk of ecosystems declining and adaptation plans failing. Under SSP5-8.5 and SSP3-7.0, the upper 5% of trends are between 0.50-0.83 °C decade⁻¹ and 0.43-0.79 °C decade⁻¹ respectively, while this extreme range is 0.32-0.50 °C decade⁻¹ for SSP1-2.6 and 0.26-0.43 °C decade⁻¹ for SSP1-1.9 (Fig. 1a; FaIR boxes). For warming rates over 0.4 °C decade⁻¹, evidence suggests that all ecosystems will decline as they will not be able to adapt rapidly enough²⁵. These extremes are caused by a combination of relatively high equilibrium climate sensitivity (ECS), high transient climate response (TCR), high effective radiative forcing (ERF) trends, and high positive internal variability. Very low near-term warming rates are also possible in all scenarios considered. However, only under mitigation would it be possible, but very unlikely, to observe a cooling trend over the next 20 years. Only 2% of trends show near-term cooling in SSP1-1.9, where the minimum trend is -0.13 °C decade⁻¹. Maher et al. (2020)⁵ found that cooling trends could be observed in the near-term even under a “worse case” emissions scenario, when using a shorter 15-year time horizon and considering trends at individual locations rather than the global average trend.

We now ask what is the probability, over the next 20 years, of the warming trend being lower if a mitigation pathway is followed rather than a no mitigation pathway. This is important since internal variability could overwhelm a forced temperature signal from diverging trajectories of greenhouse gas and aerosol concentrations, masking the near-term benefits of mitigation efforts. The probability that pursuing a mitigation pathway will result in a lower near-term temperature trend by a factor α as compared to following a no mitigation pathway ($P(\text{trend}_{\text{mit}} < \text{trend}_{\text{nomit}} - \alpha \times \text{trend}_{\text{nomit}})$) is shown in Table 1a. Values of α are chosen to assess whether the trend is, first, lower by any amount ($\alpha = 0$) and, second, lower by a sizable amount (20% and 40%, $\alpha = 0.2$ and $\alpha = 0.4$). The probabilities for $\alpha = 0$ are calculated from the distributions created by randomly sampling with replacement from each FaIR trend distribution and taking

their difference, where this is repeated $n=10^5$ times (Fig. 2a and 2b). For $\alpha = 0.2$ and $\alpha = 0.4$, the probabilities are calculated by shifting the same distributions by amount $\alpha \times \text{trend}_{\text{nomit}}$. Comparing the 1.5 °C and 2 °C scenarios (SSP1-1.9 and SSP1-2.6) to the “average” no mitigation scenario (SSP3-7.0; Fig. 2a), there is respectively around a 90% and 80% probability (Table 1a) that the near-term temperature trend would be lower when following the strong mitigation pathway. Under less ambitious mitigation consistent with current and projected NDCs, the probability of the warming trend being lower than in the “average” no mitigation pathway is 74%. Even when it is required that the trend under mitigation is at least 20% (40%) lower than under no mitigation, there is still a 83% (67%) probability of this outcome for SSP1-1.9 compared to SSP3-7.0.

A more stringent test, similar to that described by Marotzke (2019)⁴ – hereafter M19 – is to ask what is the probability that mitigation is both *sufficient* and *necessary* (P_{ns}) for a reduction in the temperature trend over 2021-2040 relative to the trend over the recent past. To calculate P_{ns} , the observed 20-year temperature trend for 2000-2019 ($\text{trend}_{\text{obs}}$) is subtracted from each distribution of FaIR near-term trends for the mitigation and no mitigation scenarios. Since the recently observed trend differs somewhat in multiple observational datasets (Supplementary Fig. 1), a dataset is randomly chosen for each comparison with the FaIR projections. The resulting distributions (Fig. 2c) give the probability of a trend reduction compared to the recent past under mitigation ($P_{\text{mit}} = P(\text{trend}_{\text{mit}} < \text{trend}_{\text{obs}})$) and no mitigation ($P_{\text{nomit}} = P(\text{trend}_{\text{nomit}} < \text{trend}_{\text{obs}})$) scenarios. P_{ns} is then calculated from $P_{\text{ns}} = P_{\text{mit}} - P_{\text{nomit}}$. This is similar to the approach of M19⁴, except that here we use the observed trend, which is known, rather than a distribution of modelled trends for the recent past. Compared to the first test conducted (Table 1a, Fig. 2a and 2b), this more stringent test gives, as expected, a lower probability of mitigation causing a reduction in the near-term temperature trend as compared to no mitigation. However, for the difference between the 1.5 °C mitigation scenario and the “average” no mitigation scenario, the

probability that mitigation is both necessary and sufficient to cause a reduction in the trend as compared to recent observations is close to a 66% probability (Table 1b).

To investigate the extent to which our results depend on the period or trend length considered, we use the FaIR emulator including estimates of internal variability to calculate warming rates for temperature trends starting in 2021 and ending in different years (Fig. 3). The 66% probability range of trends for SSP3-7.0 and SSP1-1.9 become non-overlapping after around 20 years (i.e., by around 2040). This is also around the time at which the SSP5-8.5 and SSP1-2.6 66% probability ranges become separated. For SSP3-7.0 and SSP1-2.6 it takes until around 2047 for the 66% probability distributions to no longer overlap. For periods shorter than 20 years (i.e., ending before 2040), the distributions of plausible warming trends between the scenarios are less distinguishable. The black line in Fig. 3 shows the maximum historical observed trend for different trend lengths based on the mean of the four datasets in Supplementary Fig. 1. The 66% probability range of trends starting from 2021 in SSP1-1.9 always falls below the maximum observed trend for all periods considered. In contrast, the median trend for SSP3-7.0 lies above the maximum observed trend for periods longer than around 18 years from present (i.e., ending after 2038).

The results presented here agree with those of Ciavarella et al. (2017)²⁶, where it is shown that strong mitigation markedly reduces the risk of exposure to climate extremes in the near-term in an earlier generation of climate models (CMIP5²⁷) driven by Representative Concentration Pathway (RCP²⁸) scenarios; however, their focus is on regional extremes and local warm seasons, whereas we take a global and annual mean perspective motivated by the Paris Agreement targets. Our results do differ somewhat though from the many studies that find little detectable benefit of mitigation in the near-term^{3-6,29-30}. This may reflect that these studies use model-based rather than observation-based estimates of internal variability (Supplementary Fig. 2), compare pathways with more similar radiative forcings^{4,6,29-30} (e.g., M19⁴ consider RCP2.6

versus RCP4.5, and Samset et al. (2020)⁶ focus on idealized mitigation scenarios for individual forcers rather than the combination of forcing agents in the SSPs), or because they consider shorter time horizons⁴⁻⁶ (e.g., M19⁴ analyses 15-year temperature trends; Fig. 3).

In contrast to our findings for near-term temperature trends, and in agreement with the IPCC's Fifth Assessment Report² where a different set of models and scenarios were compared, our results show little difference between SSP scenarios for mean temperature anomalies (as opposed to trends) in the next 20 years (2021-2040) relative to a baseline of 1995-2014 (Fig. 1b). This holds for both the observationally-constrained CMIP6 projections and FaIR projections with added internal variability. The median 20-year mean temperature anomalies for the different SSPs all lie within 0.62-0.71 °C for the constrained CMIP6 projections (0.55-0.70 °C for FaIR), with the range about the median being determined by internal variability, differences in climate response between models, and differences in effective radiative forcing. Differing conclusions about the detectability of differences in temperature trends and anomalies between scenarios in Fig. 1 arise because the anomalies quantify the difference in warming between the 20-year periods centered on 2030 and 2005, while the trends quantify the difference in warming between the later years of 2040 and 2021, a period for which the different emissions pathways are more divergent (Supplementary Fig. 3).

To conclude, we have shown that rapid mitigation of global greenhouse gas emissions substantially reduces the risk of experiencing unprecedented rates of surface warming over the next two decades, even after accounting for internal variability. This is in addition to the longer-term benefits of stringent mitigation for peak warming and stabilization of climate. While it is possible that unprecedented warming rates could occur in the near-term even if society pursues a path towards net-zero emissions around mid-century, the risk of such an outcome is substantially reduced by around a factor of 13 for the most ambitious mitigation scenario (SSP1-1.9) as compared to an “average” no mitigation scenario (SSP3-7.0).

The rate of warming over the next 20 years will determine the pace at which, and extent to which, society and ecosystems will need to adapt to evolving climate hazards. Based on our results, under the strong mitigation scenario SSP1-2.6 the probability of crossing the threshold of 1.5 °C of anthropogenic warming in the next 20 years is around half that in SSP3-7.0 (42% compared to 78% probability; Supplementary Table 2). Furthermore, the lower near-term warming rates under SSP1-1.9 give an estimated 74% probability that the 1.5 °C threshold will never be crossed (Supplementary Table 2). The IPCC SR1.5 report^{1,31} shows that warming of 1.5 °C is associated with severe and widespread impacts and risks from: extreme weather events (e.g., projections show extreme heatwaves becoming widespread in the tropics³²⁻³⁴; the hottest days in mid-latitudes becoming up to 3 °C warmer³⁵⁻³⁷; the coldest nights in the Arctic becoming up to 4.5 °C warmer³⁵⁻³⁷; increases in the frequency, intensity, and/or amount of heavy precipitation in several regions globally³⁵⁻³⁷); and ocean warming and acidification, which are expected to impact a range of marine organisms and ecosystems (e.g., 70-90% of warm-water coral reefs are projected to disappear at a warming of 1.5 °C³⁸). The aggregated effect of these climate impacts and risks is projected to be highest in regions where vulnerable populations live, particularly in South Asia³⁹. The results reported here serve as further motivation for setting stringent mitigation targets to reach net-zero emissions as soon as possible on both global and individual-country levels.

Lastly, it is important to communicate what can be reasonably expected from stringent mitigation in the near-term, so as to manage expectations and avoid causing doubt in the public mind about how well anthropogenic climate change is understood. In particular, while we have shown there is a high probability that stringent mitigation would result in lower near-term warming rates as compared to an “average” no mitigation scenario, there is a lower probability that stringent mitigation is necessary and sufficient to cause a slow-down in the warming rate in the near-term as compared to the recent past.

References

1. IPCC. Summary for Policymakers. In: *Global Warming of 1.5°C. An IPCC Special Report on the impacts of global warming of 1.5°C above pre-industrial levels and related global greenhouse gas emission pathways, in the context of strengthening the global response to the threat of climate change, sustainable development, and efforts to eradicate poverty* (eds Masson-Delmotte, V. et al.). 32pp (World Meteorological Organization, Geneva, Switzerland, 2018).
2. Kirtman, B. et al. Near-term Climate Change: Projections and Predictability. In: *Climate Change 2013: The Physical Science Basis. Contribution of Working Group I to the Fifth Assessment Report of the Intergovernmental Panel on Climate Change* (eds Stocker, T. F. et al.). Ch. 11, 953–1028 (Cambridge University Press, Cambridge, 2013).
3. Tebaldi, C. & Friedlingstein, P. Delayed detection of climate mitigation benefits due to climate inertia and variability. *Proc. Natl. Acad. Sci. U. S. A.* **110**, 17229–17234 (2013).
4. Marotzke, J. Quantifying the irreducible uncertainty in near-term climate projections. *WIREs Clim. Change.* **10**, e563 (2019).
5. Maher, N., Lehner, F. & Marotzke, J. Quantifying the role of internal variability in the temperature we expect to observe in the coming decades. *Environ. Res. Lett.* **15**, 054014 (2020).
6. Samset, B. H., Fuglestad, J. S. & Lund, M. T. Delayed emergence of a global temperature response after emission mitigation. *Nat. Commun.* **11**, 3261 (2020).
7. Challinor, A. et al. Current warming will reduce yields unless maize breeding and seed systems adapt immediately. *Nat. Clim. Change* **6**, 954–958 (2016).
8. Gersonius, B. et al. Managing the flooding system's resiliency to climate change. *P. I. Civil. Eng.-Eng. Su* **163**, 15–22 (2010).

9. Allen, M. R. et al. Framing and Context. In: *Global Warming of 1.5°C. An IPCC Special Report on the impacts of global warming of 1.5°C above pre-industrial levels and related global greenhouse gas emission pathways, in the context of strengthening the global response to the threat of climate change, sustainable development, and efforts to eradicate poverty* (eds Masson-Delmotte, V. et al). Ch. 1 (2018).
10. Schleussner, C.-F. et al. Science and policy characteristics of the Paris Agreement temperature goal. *Nat. Clim. Change* **6**, 827–835 (2016).
11. Rogelj, J., Schleussner, C.-F. & Hare, W. Getting it right matters: Temperature goal interpretations in geoscience research. *Geophys. Res. Lett.* **44**, 10662–10665 (2017).
12. Hawkins, E. & Sutton, R. The Potential to Narrow Uncertainty in Regional Climate Predictions. *Bull. Amer. Meteor. Soc.* **90**, 1095–1108 (2009).
13. Lehner, F. et al. Partitioning climate projection uncertainty with multiple Large Ensembles and CMIP5/6. *Earth Syst. Dynam.* **11**, 491–508 (2020).
14. Kosaka, Y. & Xie, S.-P. Recent global-warming hiatus tied to equatorial Pacific surface cooling. *Nature* **501**, 403–407 (2013).
15. Medhaug, I., Stolpe, M. B., Fischer, E. M. & Knutti, R. Reconciling controversies about the ‘global warming hiatus’. *Nature* **545**, 41–47 (2017).
16. Meinshausen, M. et al. The shared socio-economic pathway (SSP) greenhouse gas concentrations and their extensions to 2500. *Geosci. Model Dev.* **13**, 3571–3605 (2020).
17. Tokarska K. B., et al. Past warming trend constrains future warming in CMIP6 models. *Sci. Adv.* **6**, eaaz9549 (2020).
18. Smith, C. J. et al. FAIR v1.3: a simple emissions-based impulse response and carbon cycle model. *Geosci. Model Dev.* **11**, 2273–2297 (2018).
19. Haustein, K. et al. A Limited Role for Unforced Internal Variability in Twentieth-Century Warming. *J. Climate* **32**, 4893–4917 (2019).

20. Rogelj, J. et al. Understanding the origin of Paris Agreement emission uncertainties. *Nat. Commun.* **8**, 15748 (2017).
21. Rogelj, J., den Elzen, M., Huppmann, D. & Luderer, G. The Emissions Gap. In: Emissions Gap Report 2019. Ch. 3 (United Nations Environment Programme, Nairobi, Kenya, 2019).
22. Vrontisi, Z. et al. Enhancing global climate policy ambition towards a 1.5°C stabilization: a short-term multi-model assessment. *Environ. Res. Lett.* **13**, 044039 (2018).
23. Hausfather, Z. & Peters, G. P. Emissions – the ‘business as usual’ story is misleading. *Nature* **577**, 618–620 (2020).
24. Leemans, R. & Eickhout, B. Another reason for concern: regional and global impacts on ecosystems for different levels of climate change. *Global Environ. Change* **14**, 219–228 (2004).
25. Neilson, R. P. Transient ecotone response to climatic change: some conceptual and modelling approaches. *Ecol. Appl.* **3**, 385–395 (1993).
26. Ciavarella, A., Stott, P. & Lowe, J. Early benefits of mitigation in risk of regional climate extremes. *Nat. Clim. Change* **7**, 326–330 (2017).
27. Taylor, K. E., Stouffer, R. J. & Meehl, G. A. An Overview of CMIP5 and the Experiment Design. *Bull. Amer. Meteor. Soc.* **93**, 485–498 (2012).
28. Meinshausen, M. et al. The RCP greenhouse gas concentrations and their extensions from 1765 to 2300. *Clim. Change* **109**, 213–241 (2011).
29. Lehner, F., Deser, C. & Sanderson, B. M. Future risk of record-breaking summer temperatures and its mitigation. *Clim. Change* **146**, 363–375 (2018).
30. Tebaldi, C. & Wehner, M. F. Benefits of mitigation for future heat extremes under RCP4.5 compared to RCP8.5. *Clim. Change* **146**, 349–361 (2018).
31. Hoegh-Guldberg, O. et al. Impacts of 1.5°C Global Warming on Natural and Human Systems. In: *Global Warming of 1.5°C. An IPCC Special Report on the impacts of global warming of 1.5°C above pre-industrial levels and related global greenhouse gas emission*

pathways, in the context of strengthening the global response to the threat of climate change, sustainable development, and efforts to eradicate poverty (eds Masson-Delmotte, V. et al.). Ch. 3 (2018).

32. Mahlstein, I., Knutti, R., Solomon, S. & Portmann, R. W. Early onset of significant local warming in low latitude countries. *Environ. Res. Lett.* **6**, 034009 (2011).
33. Coumou, D. & Robinson, A. Historic and future increase in the global land area affected by monthly heat extremes. *Environ. Res. Lett.* **8**, 034018 (2013).
34. Dosio, A., Mentaschi, L., Fischer, E. M. & Wyser, K. Extreme heat waves under 1.5 °C and 2 °C global warming. *Environ. Res. Lett.* **13**, 054006 (2018).
35. Seneviratne, S. I., Donat, M. G., Pitman, A. J., Knutti, R. & Wilby, R. L. Allowable CO₂ emissions based on regional and impact-related climate targets. *Nature* **529**, 477–483 (2016).
36. Wartenburger, R. et al. Changes in regional climate extremes as a function of global mean temperature: an interactive plotting framework. *Geosci. Model Dev.* **10**, 3609–3634 (2017).
37. Seneviratne, S. I et al. Climate extremes, land–climate feedbacks and land-use forcing at 1.5°C. *Phil. Trans. R. Soc. A.* **376**, 20160450 (2018).
38. Schleussner, C.-F. et al. Differential climate impacts for policy-relevant limits to global warming: the case of 1.5 °C and 2 °C. *Earth Syst. Dynam.* **7**, 327–351 (2016).
39. Byers, E. Global exposure and vulnerability to multi-sector development and climate change hotspots. *Environ. Res. Lett.* **13**, 055012 (2018).

251 **Methods**

252 The global mean surface air temperature projections used in this study come from two different
 253 approaches: the Finite amplitude Impulse Response (FaIR) simple climate model emulator¹⁸,

with added observation-based estimates of internal variability¹⁹ described below, and the latest-generation comprehensive climate models from CMIP6⁴⁰ constrained by observations¹⁷. In the main text, the main results regarding temperature trends are quantified using the distributions from FaIR rather than CMIP6, since FaIR is computationally inexpensive and can therefore more broadly sample parameter uncertainty than the more complex models used in CMIP6. FaIR can also be used to explore a wider range of emission scenarios, including an NDC-like scenario (not available for CMIP6) and the most ambitious mitigation scenario, SSP1-1.9 (too few CMIP6 models were available at the time of writing to generate adequate statistics). Note the temperature trend distributions for the constrained CMIP6 models are very similar to FaIR, however, so both approaches are in good agreement. All trends were calculated using least-squares linear regression.

Finite Amplitude Impulse Response (FaIR) model

FaIR was used in the IPCC SR1.5 report⁴¹ and uses values for equilibrium climate sensitivity (ECS), transient climate response (TCR), and a time-series of effective radiative forcing (ERF) to make projections of surface temperature. Here, distributions of near-term temperature projections for FaIR were calculated using 500 simulations for each SSP and the NDC-like scenario, using distributions of ECS, TCR, and ERF that reflect our latest understanding since SR1.5.

The ECS can be defined as $-F_{2x}/\lambda$, where F_{2x} is the effective radiative forcing from a doubling of CO_2 and λ is the global climate feedback parameter. To construct a distribution of ECS we use this relationship, sampling λ from a normal distribution with mean $-1.34 \text{ W m}^{-2} \text{ K}^{-1}$ and standard deviation $0.28 \text{ W m}^{-2} \text{ K}^{-1}$, and F_{2x} equal to 4.01 W m^{-2} . This reproduces a distribution of ECS that is right-skewed (long tail which does not exclude very high ECS values) and a 5-95% range of $2\text{-}5^\circ\text{C}$ with a best estimate near 3°C (cf. ref. 42). The higher value of F_{2x} compared to the

IPCC's Fifth Assessment Report results from an updated spectroscopic relationship for stratospherically-adjusted CO₂ radiative forcing of 3.81 W m⁻² for a doubling of CO₂ (ref. 43) plus tropospheric radiative adjustments that sum to 0.20 W m⁻² (ref. 44), calculated using radiative kernels in ten climate models, and subtracting the land-surface warming component. The TCR is sampled to maintain a strong correlation with ECS⁴⁵, with a marginal distribution of TCR of 1.7 °C (1.2-2.4 °C, 5-95% range) that is broadly consistent with observational constraints¹⁷. Our sampling method allows the possibility of high ECS for modest TCR⁴⁶.

Emissions of greenhouse gases and short-lived climate forcers are taken from the Reduced Complexity Model Intercomparison Project dataset⁴⁷, which assimilate anthropogenic and natural short-lived climate forcers⁴⁸⁻⁴⁹ and inversions of greenhouse gas concentrations observed historically as well as those projected in SSP scenarios^{16,50}. The emissions used for the NDC-like pathway are representative of the scenarios described in the UNEP Emissions Gap Report 2019²¹ and also of the pathways for the NDC-like projections in ref. 22. The emissions pathways used for each SSP scenario considered and the NDC-like scenario are shown in Supplementary Fig. 3. The most ambitious (strong) mitigation scenario SSP1-1.9 (SSP1-2.6) is associated with a mitigation rate of -0.3 GtC year⁻¹ (-0.2 GtC year⁻¹) in global net CO₂ emissions from 2021 to reach net-zero emissions in 2056 (2076). This is consistent with keeping anthropogenic warming below 1.5 °C (2 °C) with a probability of 74% (92%) (Supplementary Fig. 4). These pathways are therefore equivalent to the "Below-1.5 °C" and "Lower-2 °C" pathways considered in the IPCC SR1.5 report (i.e., pathways with no or limited overshoot; see Table 2.1 in ref. 51).

Emissions of CO₂ are converted to concentrations through a simple carbon cycle representation that is temperature and carbon-uptake dependent⁵². The carbon cycle parameters that govern the atmospheric lifetime of CO₂ (pre-industrial airborne fraction, and sensitivity of airborne fraction to increasing global mean surface air temperature (GSAT) and total atmospheric carbon

burden) are sampled from Gaussian distributions¹⁶ that reproduce the observed CO₂ concentration of 407 ppm in 2018 in the ensemble median. Concentrations of non-CO₂ gases are calculated from a simple one-box model based on atmospheric lifetimes from ref. 53. Greenhouse gas ERFs are calculated from concentrations from ref. 43 for CO₂, CH₄, and N₂O, and ref. 54 for other species. To account for tropospheric rapid adjustments, CO₂ forcing is increased by 5% and CH₄ forcing reduced by 14%¹⁸, the latter case based on the behavior of tropospheric water vapor in climate models that include shortwave forcing of methane. Simple relationships that convert aerosol and ozone precursors to forcings are also employed⁵⁵⁻⁵⁷ as described in ref. 18. Noting that the default CMIP6 aerosol forcing may have resulted in too little warming over the later 20th century in some models^{47,58} with a strong warming rebound in more recent years, we repeat the analysis but substituting in the aerosol ERF time series from AR5⁵⁹. However, this makes little difference to future near-term warming rates (Supplementary Fig. 5). Volcanic forcing is determined from the CMIP6 stratospheric sulphate optical depth time-series (REF) converted to ERF at -18τ with an additive offset applied such that the mean volcanic ERF over the historical period is zero. Solar forcing is taken from the CMIP6 extraterrestrial solar flux dataset⁶⁰ using a reference time frame of 1850-1873 as recommended for CMIP6 pre-industrial control simulations. To convert solar flux anomaly to annual ERF, it is multiplied by $\frac{1}{4}$ (geometric factor) x 0.7 (planetary co-albedo).

Twelve categories of anthropogenic and natural radiative forcings are simulated using input emissions, with best estimate and uncertainties in the pre-industrial to present-day ERF taken from the IPCC's Fifth Assessment Report⁵³, with the exception being for aerosols for which the review of ref. 61 is used for the 5-95% distribution of aerosol forcing of -2.0 to -0.4 W m⁻² based on a comprehensive assessment (this range of present-day aerosol ERF is also applied to the AR5 time series in Supplementary Fig. 5). Uncertainties are applied as a fraction of the present-day forcing (see Table 3 in ref. 18). Historical (1995-2014) and projected near-term (2021-2040)

trends in the median total ERF, and its twelve components, are shown in Supplementary Table 1.

FaIR does not include internal climate variability and, therefore, the simulations described above only give the distribution of externally-forced temperature trends (Supplementary Fig. 6).

However, near-term warming trends will be significantly affected by internal variability (e.g., ref. 4). To account for this, we add an observation-based estimate of internal variability to the forced temperature trends from FaIR. To estimate internal variability from the observed record, we use the approach of a recent study¹⁹. In this approach, a two-box impulse response model (IRM) is used to calculate forced temperature changes since 1850, and this estimate is subtracted from the observational record to estimate temperature changes due to internal variability alone (Supplementary Fig. 7a and 7b). The resulting histogram of rolling trends for 20-year segments of the temperature residuals (Supplementary Fig. 7c and 7d) is then added to each of the 500 simulated temperature trends in FaIR (Supplementary Fig. 6), and a boxplot is calculated (Fig. 1a). Here we use HadOST as the observational dataset because its sea surface temperatures (SSTs) are less biased than other datasets (e.g., Berkeley Earth Land-Ocean and Cowtan-Way version 2 updated with HadSST3)¹⁹. However, the dataset used has little effect on the distributions of 20-year temperature trends due to internal variability (Supplementary Fig. 8a).

An alternative for estimating the range of temperature trends due to internal variability is to use the CMIP6 pre-industrial control simulations. Histograms of rolling temperature trends for 20-year segments of the control simulation for each of the 48 currently available CMIP6 models are shown in Supplementary Fig. 2 (see Supplementary Table 3 for a list of the models used).

Before calculating these trends, any drift in each simulation was removed by subtracting the linear trend across the whole simulation. Clearly, there are noticeable differences in the magnitude of low frequency temperature variability between models, where MIROC-ES2L is an example of a “low” variability model and BCC-CSM2-MR a “high” variability model. Adding the

histogram for MIROC-ES2L to each of the 500 FaIR temperature trends gives similar distributions to using an observation-based estimate of variability (compare Supplementary Fig. 8a with 8bi). The range of resulting trends is larger when using the “high” variability model BCC-CSM2-MR (Supplementary Fig. 8bii), but even with this high estimate of variability strong mitigation still substantially reduces the risk of unprecedented warming. Under SSP1-1.9 (SSP1-2.6), 13% (26%) of trends are above the maximum observed historical trend, while for SSP3-7.0 (SSP5-8.5) this increases to 55% (69%).

Observation-based estimates of internal variability are also added to the distributions of temperature anomalies for FaIR in Fig. 1b. To do this, we first calculate the rolling mean for 20-year segments of the temperature residuals in Supplementary Fig. 7b. We then calculate rolling differences in these 20-year means, where – to preserve autocorrelation – the temporal separation between each pair of 20-year means is consistent with the separation between 2021-2040 and 1995-2014. The resulting histogram of differences in 20-year means of residuals is then added to the forced temperature anomalies from FaIR.

Note that the residuals in Supplementary Fig. 7b do not include natural variability due to volcanic and solar forcing, since ref. 19 includes volcanic and solar forcing in the IRM simulations of historical temperatures. Estimated future solar variability is included in the ERF time-series used to make the FaIR GSAT projections, but forcing from possible future volcanic eruptions is not. It is therefore acknowledged that if, in the near-term, solar variability is different from estimated or a large volcanic eruption occurs, near-term temperature trends will be different from those reported here.

Coupled Model Intercomparison Project Phase 6 (CMIP6) models

We now describe the estimates of near-term warming trends derived from the CMIP6 models. It has been reported that some CMIP6 models simulate higher ECS values than previous versions

in CMIP5, with some models simulating an ECS of up to around 5.7 °C (e.g., ref. 62). Projected raw warming rates in those models may be higher than in the past⁶² and inconsistent with recent observed warming rates¹⁷. Additional information can be used to constrain a multi-model ensemble using so-called emergent constraints. Several studies have recently applied constraints to the CMIP6 multi-model ensemble global temperature projections using observed warming rates over the past few decades as compared to the models' "historical" simulations^{17,58,63-64}. Here, we use the approach of ref. 17, which applies an emergent constraint on the CMIP6 model spread based on the relationship between the surface warming rate over 1981-2017 and projected future warming levels ($R = 0.92$ and $R = 0.86$ for mid- and end-of-century, respectively, for SSP5-8.5). This justifies using the present-day observational trend estimates to constrain future projections. The observationally-constrained CMIP6 median warming is over 10% lower by 2050 compared to the raw CMIP6 median, and over 17% lower by 2100¹⁷. Constrained CMIP6 projections were not provided for SSP1-1.9 because at the time of writing not enough models were available to apply the emergent constraint based on past warming rates.

A list of the CMIP6 models used to derive the constrained temperature trends can be found in Supplementary Table 3 (see Supplementary Table S1 in ref. 17 for a more detailed list of models used in each SSP scenario).

Observation-based surface temperature datasets

To calculate observation-based temperature trends over the historical period we use four different datasets: HadCRUT4.6.0.0 (HadCRUT4.6⁶⁵); Berkeley Earth Land-Ocean (BE⁶⁶); Cowtan-Way version 2 updated with HadSST3 (CWv2⁶⁷⁻⁷⁰); and GISTEMP version 4 (GISTEMPv4⁷¹⁻⁷²).

The observation-based datasets report global mean historical surface temperature anomalies, calculated using a blend of land near-surface air temperatures and SSTs (referred to here as global blended surface temperature, GBST¹⁷). Over land, HadCRUT4.6 and CWv2 use CRUTEM4⁷³; BE uses the Berkeley Earth land-surface temperature field; and GISTEMPv4 uses NOAA GHCN v4⁷⁴. Over ocean, HadSST is used for HadCRUT4.6, CWv2, and BE; and GISTEMPv4 uses ERSSTv5⁷⁵. BE, CWv2, and GISTEMPv4 are interpolated to near-full coverage, while HadCRUT4.6 is left un-interpolated and therefore has incomplete coverage. By using several datasets, we aim to ensure the results are not biased towards any one combination of land and ocean data.

We report CMIP6 and FaIR model results in terms of the global mean near-surface air temperature (GSAT), since this is most relevant for future climate projections and impact assessments⁷⁶. Since the observation-based GBST metric has been warming slower on average than GSAT⁷⁷, we apply a scaling factor to GBST that accounts for the blending bias and converts it to a GSAT equivalent, therefore allowing a like-for-like comparison between the observations and models. We use $GSAT = 1.087 \times GBST$ for BE, CWv2, and GISTEMPv4; and $GSAT = 1.19 \times GBST$ for HadCRUT4.6. These scaling factors are based on estimates derived from the CMIP5 models for fully-blended GBST (applicable to BE, CWv2, and GISTEMPv4) and blended-masked GBST (applicable to HadCRUT4.6); see Table 1 in ref. 78, and Supplementary Fig. 1 in ref. 79. Note that the results reported in this study are, however, relatively insensitive to the exact scaling factor applied.

To calculate the observation-based estimates of internal variability in 20-year temperature trends (Supplementary Fig. 7), we use the same datasets as in ref. 19: CWv2 (updated with HadSST4⁸⁰ here), BE, and HadOST¹⁹. HadOST combines CWv2 over land with HadISST2⁸¹ and OSTIA⁸² data over ocean, and is interpolated to near-full coverage. To convert HadOST to a GSAT equivalent, we use the scaling factor for fully-blended GBST (1.087). To account for a

warm bias in SSTs around 1942-1945 due to changing SST sampling methods, correction factors have been applied over these years to the observation-based datasets in Supplementary Fig. 7 as in ref. 19.

Data availability

The data that support the findings of this study are available at [https://github.com/Priestley-Centre/Near_term_warming] with the identifier [<https://doi.org/10.5281/zenodo.3762042>]⁸³. This repository includes the FaIR simulation data, the constrained CMIP6 projections, the observation-based data, and the observation-based estimates of internal variability (in fully processed form only). The SSP emissions datasets used in the FaIR simulations were downloaded from [<https://www.rcmip.org/>], and the NDCs emissions dataset was provided by Joeri Rogelj. The constrained CMIP6 projections are based on ref. 17 and used surface air temperature data downloaded from ESGF (Dec 4 2019). The raw data used to calculate the observation-based estimates of internal variability are based on ref. 19, and were provided by Karsten Haustein. Surface air temperature data for the CMIP6 pre-industrial control simulations were obtained from the JASMIN/CEDA archive (Jul 29 2020).

Code availability

The FaIR model is available from [<https://doi.org/10.5281/zenodo.3588880>]⁸⁴. FaIR version 1.5 is used for all simulations in this paper. The code used to setup the FaIR simulations, analyze data, and produce figures is available at [https://github.com/Priestley-Centre/Near_term_warming] with the identifier [<https://doi.org/10.5281/zenodo.3762042>]⁸³. Python/Matplotlib was used for all coding and data visualization, and for some figures the vector

446 graphics editor Inkscape (available at [<https://inkscape.org/>]) was used to combine different
447 figure parts into one file.

References

40. Eyring, V. et al. Overview of the Coupled Model Intercomparison Project Phase 6 (CMIP6) experimental design and organization. *Geosci. Model Dev.* **9**, 1937–1958 (2016).
41. IPCC. *Global Warming of 1.5°C. An IPCC Special Report on the impacts of global warming of 1.5°C above pre-industrial levels and related global greenhouse gas emission pathways, in the context of strengthening the global response to the threat of climate change, sustainable development, and efforts to eradicate poverty* (eds Masson-Delmotte, V. et al.). (2018).
42. Dessler, A. E. & Forster, P. M. An estimate of equilibrium climate sensitivity from interannual variability. *J. Geophys. Res. Atmos.* **123**, 8634–8645 (2018).
43. Etminan, M., Myhre, G., Highwood, E. J. & Shine, K. P. Radiative forcing of carbon dioxide, methane, and nitrous oxide: a significant revision of the methane radiative forcing. *Geophys. Res. Lett.* **43**, 12614–12623 (2016).
44. Smith, C. J. et al. Understanding rapid adjustments to diverse forcing agents. *Geophys. Res. Lett.* **45**, 12023–12031 (2018).
45. Flato, G. et al. Evaluation of Climate Models. In: *Climate Change 2013: The Physical Science Basis. Contribution of Working Group I to the Fifth Assessment Report of the Intergovernmental Panel on Climate Change* (eds Stocker, T. F. et al.). Ch. 9 (Cambridge University Press, 2013).
46. Pfister, P. L. & Stocker, T. F. The realized warming fraction: a multi-model sensitivity study. *Environ. Res. Lett.* **13**, 124024 (2018).

47. Nicholls, Z. R. et al. Reduced complexity model intercomparison project phase 1: Protocol, results and initial observations. *Geosci. Model Dev. Discuss.*, <https://doi.org/10.5194/gmd-2019-375>, in press (2020).
48. van Marle, M. J. E. et al. Historic global biomass burning emissions for CMIP6 (BB4CMIP) based on merging satellite observations with proxies and fire models (1750–2015). *Geosci. Model Dev.* **10**, 3329–3357 (2017).
49. Hoesly, R. M. et al. Historical (1750–2014) anthropogenic emissions of reactive gases and aerosols from the Community Emissions Data System (CEDS). *Geosci. Model Dev.* **11**, 369–408 (2018).
50. Meinshausen, M. et al. Historical greenhouse gas concentrations for climate modelling (CMIP6). *Geosci. Model Dev.* **10**, 2057–2116 (2017).
51. Rogelj, J. et al. Mitigation Pathways Compatible with 1.5°C in the Context of Sustainable Development. In: *Global Warming of 1.5°C. An IPCC Special Report on the impacts of global warming of 1.5°C above pre-industrial levels and related global greenhouse gas emission pathways, in the context of strengthening the global response to the threat of climate change, sustainable development, and efforts to eradicate poverty* (eds. Masson-Delmotte, V. et al.). Ch. 2 (2018).
52. Millar, R. J., Nicholls, Z. R., Friedlingstein, P. & Allen, M. R. A modified impulse-response representation of the global near-surface air temperature and atmospheric concentration response to carbon dioxide emissions. *Atmos. Chem. Phys.* **17**, 7213–7228 (2017).
53. Myhre, G. et al. Anthropogenic and Natural Radiative Forcing. In: *Climate Change 2013: The Physical Science Basis. Contribution of Working Group I to the Fifth Assessment Report of the Intergovernmental Panel on Climate Change* (eds Stocker, T. F. et al.). Ch. 8 (Cambridge University Press, Cambridge, 2013).
54. Hodnebrog, Ø. et al. Global warming potentials and radiative efficiencies of halocarbons and related compounds: A comprehensive review. *Rev. Geophys.* **51**, 300–378, (2013).

55. Stevenson, D. S. et al. Tropospheric ozone changes, radiative forcing and attribution to emissions in the Atmospheric Chemistry and Climate Model Intercomparison Project (ACCMIP). *Atmos. Chem. Phys.* **13**, 3063–3085 (2013).
56. Myhre, G. et al. Radiative forcing of the direct aerosol effect from AeroCom Phase II simulations. *Atmos. Chem. Phys.* **13**, 1853–1877 (2013).
57. Ghan, S. J. et al. A simple model of global aerosol indirect effects. *J. Geophys. Res. Atmos.* **118**, 6688–6707 (2013).
58. Flynn, C. M. & Mauritsen, T. On the Climate Sensitivity and Historical Warming Evolution in Recent Coupled Model Ensembles. *Atmos. Chem. Phys. Discuss.* **20**, 7829–7842 (2020).
59. IPCC. Annex II: Climate System Scenario Tables (eds Prather, M. et al.). In: *Climate Change 2013: The Physical Science Basis. Contribution of Working Group I to the Fifth Assessment Report of the Intergovernmental Panel on Climate Change* (eds Stocker, T. F. et al.). (Cambridge University Press, Cambridge, 2013).
60. Matthes, K. et al. Solar forcing for CMIP6 (v3.2). *Geosci. Model Dev.* **10**, 2247–2302 (2017).
61. Bellouin, N. et al. Bounding global aerosol radiative forcing of climate change. *Reviews of Geophysics* **57**, e2019RG000660 (2019).
62. Forster, P. M., Maycock, A. C., McKenna, C. M. & Smith, C. J. Latest climate models confirm need for urgent mitigation, *Nat. Clim. Change* **10**, 7–10 (2020).
63. Jiménez-de-la-Cuesta, D. & Mauritsen, T. Emergent constraints on Earth’s transient and equilibrium response to doubled CO₂ from post-1970s global warming. *Nat. Geosci.* **12**, 902–905 (2019).
64. Nijse, F. J. M. M., Cox, P. M. & Williamson, M. S. Emergent constraints on transient climate response (TCR) and equilibrium climate sensitivity (ECS) from historical warming in CMIP5 and CMIP6 models. *Earth Syst. Dynam.* **11**, 737–750 (2020).

65. Morice, C. P., Kennedy, J. J., Rayner, N. A. & Jones, P. D. Quantifying uncertainties in global and regional temperature change using an ensemble of observational estimates: The HadCRUT4 dataset. *J. Geophys. Res.* **117**, D08101 (2012).
66. Rohde, R. et al. A new estimate of the average Earth surface land temperature spanning 1753 to 2011. *Geoinfo. Geostat. Overview* **1** (2013).
67. Kennedy, J. J., Rayner, N. A., Smith, R. O., Saunby, M. & Parker, D. E. Reassessing biases and other uncertainties in sea-surface temperature observations since 1850: 1. Measurement and sampling errors. *J. Geophys. Res.* **116**, D14103 (2011).
68. Kennedy, J. J., Rayner, N. A., Smith, R. O., Saunby, M. & Parker, D. E. Reassessing biases and other uncertainties in sea-surface temperature observations since 1850: 2. Biases and homogenisation. *J. Geophys. Res.* **116**, D14104 (2011).
69. Cowtan, K. & Way, R. G. Coverage bias in the HadCRUT4 temperature series and its impact on recent temperature trends. *Q. J. R. Meteorol. Soc.* **140**, 1935–1944 (2014).
70. Cowtan, K. D. & Way, R. G. *Global temperature reconstructions version 2 (Cowtan and Way)*. Dataset accessed at: <https://doi.org/10.15124/20ee85c3-f53c-4ab6-8e50-270b0ddd3686> (2020-02-07).
71. Lenssen, N. et al. Improvements in the GISTEMP uncertainty model. *J. Geophys. Res. Atmos.* **124**, 6307–6326 (2019).
72. GISTEMP Team. *GISS Surface Temperature Analysis (GISTEMP), version 4*. NASA Goddard Institute for Space Studies. Dataset accessed at: <https://data.giss.nasa.gov/gistemp/> (2020-01-28).
73. Jones, P. D. et al. Hemispheric and large-scale land surface air temperature variations: An extensive revision and an update to 2010. *J. Geophys. Res.* **117** (2012).
74. Menne, M. J., Williams, C. N., Gleason, B. E., Rennie, J. J. & Lawrimore, J. H. The Global Historical Climatology Network Monthly Temperature Dataset, Version 4. *J. Climate* **31**, 9835–9854 (2018).

75. Huang, B. et al. Extended Reconstructed Sea Surface Temperature, Version 5 (ERSSTv5): Upgrades, Validations, and Intercomparisons. *J. Climate* **30**, 8179–8205 (2017).
76. Tokarska, K. B. et al. Recommended temperature metrics for carbon budget estimates, model evaluation and climate policy. *Nat. Geosci.* **12**, 964–971 (2019).
77. Cowtan, K. et al. Robust comparison of climate models with observations using blended land air and ocean sea surface temperatures, *Geophys. Res. Lett.* **42**, 6526–6534 (2015).
78. Richardson, M., Cowtan, K. & Millar, R. J. Global temperature definition affects achievement of long-term climate goals. *Environ. Res. Lett.* **13**, 054004 (2018).
79. Rogelj, J., Forster, P. M., Kriegler, E., Smith, C. J. & Séférian, R. Estimating and tracking the remaining carbon budget for stringent climate targets. *Nature* **571**, 335–342 (2019).
80. Kennedy, J. J., Rayner, N. A., Atkinson, C. P. & Killick, R. E. An ensemble data set of sea-surface temperature change from 1850: the Met Office Hadley Centre HadSST.4.0.0.0 data set. *J. Geophys. Res. Atmos.* **124** (2019).
81. Titchner, H. & Rayner, N. The Met Office Hadley Centre sea ice and sea surface temperature data set, version 2: 1. Sea ice concentrations. *J. Geophys. Res.* **119**, 2864–2889 (2014).
82. Donlon, C. J. et al. The Operational Sea Surface Temperature and Sea Ice Analysis (OSTIA) system. *Remote Sens. Environ.* **116**, 140–158 (2012).
83. McKenna, C. M., Forster, P. M., Maycock, A. C., Smith, C. J. & Tokarska, K. B.. Priestley-Centre/Near_term_warming (Version v1.1). <https://doi.org/10.5281/zenodo.3762042> (Zenodo, 2020).
84. chrisroadmap, Gieseke, R. & Nicholls, Z. OMS-NetZero/FAIR: RCMIP phase 1 (Version v1.5). <https://doi.org/10.5281/zenodo.3588880> (Zenodo, 2019).
85. Haustein, K. et al. A real-time Global Warming Index. *Sci. Rep.* **7**, 15417 (2017).

86. Smith, T. M., Reynolds, R. W., Peterson, T. C. & Lawrimore, J. Improvements to NOAA's Historical Merged Land–Ocean Surface Temperatures Analysis (1880–2006). *J. Climate* **21**, 2283–2296 (2008).
87. Vose, R. S. et al. NOAA's merged land-ocean surface temperature analysis. *Bull. Amer. Meteor. Soc.* **93**, 1677–1685 (2012).
- 448 88. Dix, M. et al. *CSIRO-ARCCSS ACCESS-CM2 model output prepared for CMIP6 CMIP*
449 *piControl*. Version 20200729. Earth System Grid Federation.
450 <https://doi.org/10.22033/ESGF/CMIP6.4311> (2019).
- 451 89. Ziehn, T. et al. *CSIRO ACCESS-ESM1.5 model output prepared for CMIP6 CMIP*
452 *piControl*. Version 20200729. Earth System Grid Federation.
453 <https://doi.org/10.22033/ESGF/CMIP6.4312> (2019).
- 454 90. Semmler, T. et al. *AWI AWI-CM1.1MR model output prepared for CMIP6 CMIP piControl*.
455 Version 20200729. Earth System Grid Federation.
456 <https://doi.org/10.22033/ESGF/CMIP6.2777> (2018).
- 457 91. Danek, C. et al. *AWI AWI-ESM1.1LR model output prepared for CMIP6 CMIP piControl*.
458 Version 20200729. Earth System Grid Federation.
459 <https://doi.org/10.22033/ESGF/CMIP6.9335> (2020).
- 460 92. Wu, T. et al. *BCC BCC-CSM2MR model output prepared for CMIP6 CMIP piControl*.
461 Version 20200729. Earth System Grid Federation.
462 <https://doi.org/10.22033/ESGF/CMIP6.3016> (2018).
- 463 93. Xin, X. et al. *BCC BCC-CSM2MR model output prepared for CMIP6 ScenarioMIP*.
464 Version 20191204. Earth System Grid Federation.
465 <https://doi.org/10.22033/ESGF/CMIP6.1732> (2019).
- 466 94. Zhang, J. et al. *BCC BCC-ESM1 model output prepared for CMIP6 CMIP piControl*.
467 Version 20200729. Earth System Grid Federation.
468 <https://doi.org/10.22033/ESGF/CMIP6.3017> (2018).

- 469 95. Rong, X. *CAMS CAMS_CSM1.0 model output prepared for CMIP6 CMIP piControl*.
470 Version 20200729. Earth System Grid Federation.
471 <https://doi.org/10.22033/ESGF/CMIP6.9797> (2019).
- 472 96. Rong, X. *CAMS CAMS-CSM1.0 model output prepared for CMIP6 ScenarioMIP*. Version
473 20191204. Earth System Grid Federation. <https://doi.org/10.22033/ESGF/CMIP6.11004>
474 (2019).
- 475 97. Swart, N. C. et al. *CCCma CanESM5 model output prepared for CMIP6 CMIP piControl*.
476 Version 20200729. Earth System Grid Federation.
477 <https://doi.org/10.22033/ESGF/CMIP6.3673> (2019).
- 478 98. Swart, N. C. et al. *CCCma CanESM5 model output prepared for CMIP6 ScenarioMIP*.
479 Version 20191204. Earth System Grid Federation.
480 <https://doi.org/10.22033/ESGF/CMIP6.1317> (2019).
- 481 99. Danabasoglu, G., Lawrence, D., Lindsay, K., Lipscomb, W. & Strand, G. *NCAR CESM2*
482 *model output prepared for CMIP6 CMIP piControl*. Version 20200729. Earth System Grid
483 Federation. <https://doi.org/10.22033/ESGF/CMIP6.7733> (2019).
- 484 100. Danabasoglu, G. *NCAR CESM2 model output prepared for CMIP6 ScenarioMIP*. Version
485 20191204. Earth System Grid Federation. <https://doi.org/10.22033/ESGF/CMIP6.2201>
486 (2019).
- 487 101. Danabasoglu, G. *NCAR CESM2-FV2 model output prepared for CMIP6 CMIP piControl*.
488 Version 20200729. Earth System Grid Federation.
489 <https://doi.org/10.22033/ESGF/CMIP6.11301> (2019).
- 490 102. Danabasoglu, G. *NCAR CESM2-WACCM model output prepared for CMIP6 CMIP*
491 *piControl*. Version 20200729. Earth System Grid Federation.
492 <https://doi.org/10.22033/ESGF/CMIP6.10094> (2019).

493 103. Danabasoglu, G. *NCAR CESM2-WACCM model output prepared for CMIP6*
494 *ScenarioMIP*. Version 20191204. Earth System Grid Federation.
495 <https://doi.org/10.22033/ESGF/CMIP6.10026> (2019).

496 104. Danabasoglu, G. *NCAR CESM2-WACCM-FV2 model output prepared for CMIP6 CMIP*
497 *piControl*. Version 20200729. Earth System Grid Federation.
498 <https://doi.org/10.22033/ESGF/CMIP6.11302> (2019).

499 105. Voldoire, A. *CMIP6 simulations of the CNRM-CERFACS based on CNRM-CM6-1 model*
500 *for CMIP experiment piControl*. Version 20200729. Earth System Grid Federation.
501 <https://doi.org/10.22033/ESGF/CMIP6.4163> (2018).

502 106. Voldoire, A. *CNRM-CERFACS CNRM-CM6-1 model output prepared for CMIP6*
503 *ScenarioMIP*. Version 20191204. Earth System Grid Federation.
504 <https://doi.org/10.22033/ESGF/CMIP6.1384> (2019).

505 107. Voldoire, A. *CNRM-CERFACS CNRM-CM6-1-HR model output prepared for CMIP6*
506 *CMIP piControl*. Version 20200729. Earth System Grid Federation.
507 <https://doi.org/10.22033/ESGF/CMIP6.4164> (2019).

508 108. Seferian, R. *CNRM-CERFACS CNRM-ESM2-1 model output prepared for CMIP6 CMIP*
509 *piControl*. Version 20200729. Earth System Grid Federation.
510 <https://doi.org/10.22033/ESGF/CMIP6.4165> (2018).

511 109. Seferian, R. *CNRM-CERFACS CNRM-ESM2-1 model output prepared for CMIP6*
512 *ScenarioMIP*. Version 20191204. Earth System Grid Federation.
513 <https://doi.org/10.22033/ESGF/CMIP6.1395> (2019).

514 110. Bader, D. C., Leung, R., Taylor, M. & McCoy, R. B. *E3SM-Project E3SM1.0 model output*
515 *prepared for CMIP6 CMIP piControl*. Version 20200729. Earth System Grid Federation.
516 <https://doi.org/10.22033/ESGF/CMIP6.4499> (2018).

- 517 111. Bader, D. C., Leung, R., Taylor, M. & McCoy, R. B. *E3SM-Project E3SM1.1 model output*
518 *prepared for CMIP6 CMIP piControl*. Version 20200729. Earth System Grid Federation.
519 <https://doi.org/10.22033/ESGF/CMIP6.11489> (2019).
- 520 112. Bader, D. C., Leung, R., Taylor, M. & McCoy, R. B. *E3SM-Project E3SM1.1ECA model*
521 *output prepared for CMIP6 CMIP piControl*. Version 20200729. Earth System Grid
522 Federation. <https://doi.org/10.22033/ESGF/CMIP6.11490> (2019).
- 523 113. EC-Earth Consortium (EC-Earth). *EC-Earth-Consortium EC-Earth3 model output*
524 *prepared for CMIP6 ScenarioMIP*. Version 20191204. Earth System Grid Federation.
525 <https://doi.org/10.22033/ESGF/CMIP6.251> (2019).
- 526 114. EC-Earth Consortium (EC-Earth). *EC-Earth-Consortium EC-Earth3-Veg model output*
527 *prepared for CMIP6 ScenarioMIP*. Version 20191204. Earth System Grid Federation.
528 <https://doi.org/10.22033/ESGF/CMIP6.727> (2019).
- 529 115. YU, Y. *CAS FGOALS-f3-L model output prepared for CMIP6 CMIP piControl*. Version
530 20200729. Earth System Grid Federation. <https://doi.org/10.22033/ESGF/CMIP6.3447>
531 (2019).
- 532 116. YU, Y. *CAS FGOALS-f3-L model output prepared for CMIP6 ScenarioMIP*. Version
533 20191204. Earth System Grid Federation. <https://doi.org/10.22033/ESGF/CMIP6.2046>
534 (2019).
- 535 117. Li, L. *CAS FGOALS-g3 model output prepared for CMIP6 CMIP piControl*. Version
536 20200729. Earth System Grid Federation. <https://doi.org/10.22033/ESGF/CMIP6.3448>
537 (2019).
- 538 118. Song, Z. et al. *FIO-QLNM FIO-ESM2.0 model output prepared for CMIP6 CMIP piControl*.
539 Version 20200729. Earth System Grid Federation.
540 <https://doi.org/10.22033/ESGF/CMIP6.9205> (2019).
- 541 119. Guo, H. et al. *NOAA-GFDL GFDL-CM4 model output piControl*. Version 20200729. Earth
542 System Grid Federation. <https://doi.org/10.22033/ESGF/CMIP6.8666> (2018).

543 120. Guo, H. et al. *NOAA-GFDL GFDL-CM4 model output prepared for CMIP6 ScenarioMIP*.
544 Version 20191204. Earth System Grid Federation.
545 <https://doi.org/10.22033/ESGF/CMIP6.9242> (2018).

546 121. Krasting, J. P. et al. *NOAA-GFDL GFDL-ESM4 model output prepared for CMIP6 CMIP*
547 *piControl*. Version 20200729. Earth System Grid Federation.
548 <https://doi.org/10.22033/ESGF/CMIP6.8669> (2018).

549 122. John, J. G. et al. *NOAA-GFDL GFDL-ESM4 model output prepared for CMIP6*
550 *ScenarioMIP*. Version 20191204. Earth System Grid Federation.
551 <https://doi.org/10.22033/ESGF/CMIP6.1414> (2018).

552 123. NASA Goddard Institute for Space Studies (NASA/GISS). *NASA-GISS GISS-E2.1G*
553 *model output prepared for CMIP6 CMIP piControl*. Version 20200729. Earth System Grid
554 Federation. <https://doi.org/10.22033/ESGF/CMIP6.7380> (2018).

555 124. NASA Goddard Institute for Space Studies (NASA/GISS). *NASA-GISS GISS-E2-1-G-CC*
556 *model output prepared for CMIP6 CMIP piControl*. Version 20200729. Earth System Grid
557 Federation. <https://doi.org/10.22033/ESGF/CMIP6.11856> (2019).

558 125. NASA Goddard Institute for Space Studies (NASA/GISS). *NASA-GISS GISS-E2.1H*
559 *model output prepared for CMIP6 CMIP piControl*. Version 20200729. Earth System Grid
560 Federation. <https://doi.org/10.22033/ESGF/CMIP6.7381> (2018).

561 126. NASA Goddard Institute for Space Studies (NASA/GISS). *NASA-GISS GISS-E2-2-G*
562 *model output prepared for CMIP6 CMIP piControl*. Version 20200729. Earth System Grid
563 Federation. <https://doi.org/10.22033/ESGF/CMIP6.7382> (2019).

564 127. Ridley, J., Menary, M., Kuhlbrodt, T., Andrews, M. & Andrews, T. *MOHC HadGEM3-*
565 *GC31-LL model output prepared for CMIP6 CMIP piControl*. Version 20200729. Earth
566 System Grid Federation. <https://doi.org/10.22033/ESGF/CMIP6.6294> (2018).

128. Ridley, J., Menary, M., Kuhlbrodt, T., Andrews, M. & Andrews, T. *MOHC HadGEM3-GC31-MM model output prepared for CMIP6 CMIP piControl*. Version 20200729. Earth System Grid Federation. <https://doi.org/10.22033/ESGF/CMIP6.6297> (2019).
129. Raghavan, K. & Panickal, S. *CCCR-IITM IITM-ESM model output prepared for CMIP6 CMIP piControl*. Version 20200729. Earth System Grid Federation. <https://doi.org/10.22033/ESGF/CMIP6.3710> (2019).
130. Volodin, E. et al. *INM INM-CM4-8 model output prepared for CMIP6 CMIP piControl*. Version 20200729. Earth System Grid Federation. <https://doi.org/10.22033/ESGF/CMIP6.5080> (2019).
131. Volodin, E. et al. *INM INM-CM4-8 model output prepared for CMIP6 ScenarioMIP*. Version 20191204. Earth System Grid Federation. <https://doi.org/10.22033/ESGF/CMIP6.12321> (2019).
132. Volodin, E. et al. *INM INM-CM5-0 model output prepared for CMIP6 CMIP piControl*. Version 20200729. Earth System Grid Federation. <https://doi.org/10.22033/ESGF/CMIP6.5081> (2019).
133. Volodin, E. et al. *INM INM-CM5-0 model output prepared for CMIP6 ScenarioMIP*. Version 20191204. Earth System Grid Federation. <https://doi.org/10.22033/ESGF/CMIP6.12322> (2019).
134. Boucher, O., Denvil, S., Caubel, A. & Foujols, M. A. *IPSL IPSL-CM6A-LR model output prepared for CMIP6 CMIP piControl*. Version 20200729. Earth System Grid Federation. <https://doi.org/10.22033/ESGF/CMIP6.5251> (2018).
135. Boucher, O., Denvil, S., Caubel, A. & Foujols, M. A. *IPSL IPSL-CM6A-LR model output prepared for CMIP6 ScenarioMIP*. Version 20191204. Earth System Grid Federation. <https://doi.org/10.22033/ESGF/CMIP6.1532> (2019).
136. Stouffer, R. *UA MCM-UA-1-0 model output prepared for CMIP6 CMIP piControl*. Earth System Grid Federation. <https://doi.org/10.22033/ESGF/CMIP6.8890> (2019).

593 137. Hajima, T. et al. *MIROC MIROC-ES2L model output prepared for CMIP6 CMIP piControl*.
594 Version 20200729. Earth System Grid Federation.
595 <https://doi.org/10.22033/ESGF/CMIP6.5710> (2019).

596 138. Tachiiri, K. et al. *MIROC MIROC-ES2L model output prepared for CMIP6 ScenarioMIP*.
597 Version 20191204. Earth System Grid Federation.
598 <https://doi.org/10.22033/ESGF/CMIP6.936> (2019).

599 139. Tatebe, H. & Watanabe, M. *MIROC MIROC6 model output prepared for CMIP6 CMIP*
600 *piControl*. Version 20200729. Earth System Grid Federation.
601 <https://doi.org/10.22033/ESGF/CMIP6.5711> (2018).

602 140. Shiogama, H., Abe, M. & Tatebe, H. *MIROC MIROC6 model output prepared for CMIP6*
603 *ScenarioMIP*. Version 20191204. Earth System Grid Federation.
604 <https://doi.org/10.22033/ESGF/CMIP6.898> (2019).

605 141. Neubauer, D. et al. *HAMMOZ-Consortium MPI-ESM1.2-HAM model output prepared for*
606 *CMIP6 CMIP piControl*. Version 20200729. Earth System Grid Federation.
607 <https://doi.org/10.22033/ESGF/CMIP6.5037> (2019).

608 142. Jungclaus, J. et al. *MPI-M MPI-ESM1.2-HR model output prepared for CMIP6 CMIP*
609 *piControl*. Version 20200729. Earth System Grid Federation.
610 <https://doi.org/10.22033/ESGF/CMIP6.6674> (2019).

611 143. Schupfner, M. et al. *DKRZ MPI-ESM1.2-HR model output prepared for CMIP6*
612 *ScenarioMIP*. Version 20191204. Earth System Grid Federation.
613 <https://doi.org/10.22033/ESGF/CMIP6.2450> (2019).

614 144. Wieners, K.-H. et al. *MPI-M MPI-ESM1.2-LR model output prepared for CMIP6 CMIP*
615 *piControl*. Version 20200729. Earth System Grid Federation.
616 <https://doi.org/10.22033/ESGF/CMIP6.6675> (2019).

617 145. Yukimoto, S. et al. *MRI MRI-ESM2.0 model output prepared for CMIP6 CMIP piControl*.
618 Version 20200729. Earth System Grid Federation.
619 <https://doi.org/10.22033/ESGF/CMIP6.6900> (2019).

620 146. Yukimoto, S. et al. *MRI MRI-ESM2.0 model output prepared for CMIP6 ScenarioMIP*.
621 Version 20191204. Earth System Grid Federation.
622 <https://doi.org/10.22033/ESGF/CMIP6.638> (2019).

623 147. Cao, J. & Wang, B. *NUIST NESMv3 model output prepared for CMIP6 CMIP piControl*.
624 Version 20200729. Earth System Grid Federation.
625 <https://doi.org/10.22033/ESGF/CMIP6.8776> (2019).

626 148. Cao, J. *NUIST NESMv3 model output prepared for CMIP6 ScenarioMIP*. Version
627 20191204. Earth System Grid Federation. <https://doi.org/10.22033/ESGF/CMIP6.2027>
628 (2019).

629 149. Bethke, I. et al. *NCC NorCPM1 model output prepared for CMIP6 CMIP piControl*.
630 Version 20200729. Earth System Grid Federation.
631 <https://doi.org/10.22033/ESGF/CMIP6.10896> (2019).

632 150. Guo, C. et al. *NCC NorESM1-F model output prepared for CMIP6 CMIP piControl*.
633 Version 20200729. Earth System Grid Federation.
634 <https://doi.org/10.22033/ESGF/CMIP6.11595> (2019).

635 151. Seland, Ø. et al. *NCC NorESM2-LM model output prepared for CMIP6 CMIP piControl*.
636 Version 20200729. Earth System Grid Federation.
637 <https://doi.org/10.22033/ESGF/CMIP6.8217> (2019).

638 152. Bentsen, M. et al. *NCC NorESM2-MM model output prepared for CMIP6 CMIP piControl*.
639 Version 20200729. Earth System Grid Federation.
640 <https://doi.org/10.22033/ESGF/CMIP6.8221> (2019).

153. Park, S. & Shin, J. *SNU SAM0-UNICON model output prepared for CMIP6 CMIP piControl*. Version 20200729. Earth System Grid Federation. <https://doi.org/10.22033/ESGF/CMIP6.7791> (2019).
154. Lee, W.-L. & Liang, H.-C. *AS-RCEC TaiESM1.0 model output prepared for CMIP6 CMIP piControl*. Earth System Grid Federation. <https://doi.org/10.22033/ESGF/CMIP6.9798> (2020).
155. Tang, Y. et al. *MOHC UKESM1.0-LL model output prepared for CMIP6 CMIP piControl*. Earth System Grid Federation. <https://doi.org/10.22033/ESGF/CMIP6.6298> (2019).
156. Good, P. et al. *MOHC UKESM1.0-LL model output prepared for CMIP6 ScenarioMIP*. Version 20191204. Earth System Grid Federation. <https://doi.org/10.22033/ESGF/CMIP6.1567> (2019).

Acknowledgements

We are grateful to Joeri Rogelj for providing the NDC scenario data and to Karsten Haustein for providing the data used to calculate the observation-based estimates of internal variability. CMM, ACM, PMF, CJS and KBT were supported by the European Union's Horizon 2020 research and innovation programme under grant agreement No 820829 (CONSTRAIN project). ACM was supported by the Natural Environment Research Council (NE/M018199/1) and Leverhulme Trust. CJS was supported by a NERC/IIASA Collaborative Research Fellowship (NE/T009381/1). We acknowledge the World Climate Research Programme, which, through its Working Group on Coupled Modelling, coordinated and promoted CMIP6. We thank the climate modelling groups for producing and making available their model output, the Earth System Grid Federation (ESGF) for archiving the data and providing access, and the multiple funding agencies who support CMIP6 and ESGF.

Correspondence statement

Correspondence and requests for materials should be addressed to CMM.

Author Contributions

PMF and ACM designed the study. CMM performed the analysis and produced the figures. CJS performed the FaIR simulations. KBT provided the constrained CMIP6 projections. All authors contributed to writing the manuscript.

Competing Interests statement

The authors declare no competing interests.

Figure Legends

Figure 1: Near-term (2021-2040) global mean surface air temperature trends and anomalies relative to near present day (1995-2014) baseline. a, trends in [$^{\circ}\text{C decade}^{-1}$]; **b,** anomalies in [$^{\circ}\text{C}$]. Data are shown for pathways consistent with: current and projected Nationally Determined Contributions (NDCs, grey box); highest ambition mitigation in line with the Paris Agreement target to pursue efforts to keep warming to below 1.5°C (SSP1-1.9, green box); strong mitigation in line with the Paris Agreement target to keep warming below 2°C (SSP1-2.6, blue boxes); “average” no policy baseline scenario (SSP3-7.0, orange boxes); and unlikely “worst case” no mitigation scenario (SSP5-8.5, brown boxes). Lighter shading shows CMIP6 projections with a historical constraint applied, and darker shading shows FaIR projections plus an observation-based estimate of internal variability (see Methods). Boxes denote the 17-83% range (66% probability) and whiskers denote the 5-95% range (90%

probability) of projections. Maximum and minimum values are shown as crosses. The maximum trend for 20-year segments of the observation-based record is $0.27\text{ }^{\circ}\text{C decade}^{-1}$ (red ticks on y-axes) based on the mean of four datasets, with a range across datasets of $0.25 - 0.29\text{ }^{\circ}\text{C decade}^{-1}$ (grey horizontal bar; $0.25\text{ }^{\circ}\text{C decade}^{-1}$ for 2000-2019 in GISTEMPv4, $0.26\text{ }^{\circ}\text{C decade}^{-1}$ for 1984-2003 in CWv2 and BE, and $0.29\text{ }^{\circ}\text{C decade}^{-1}$ for 1984-2003 in HadCRUT4.6; see Supplementary Fig. 1). To compare with the model simulated GSAT projections, the observation data have been converted from GBST to GSAT using a scaling factor of 1.087 for BE, CWv2, and GISTEMPv4, and 1.19 for HadCRUT4.6 (see Methods).

Figure 2: The effect of mitigation versus no mitigation on near-term (2021-2040) global mean surface air temperature trend distributions from FaIR [$^{\circ}\text{C decade}^{-1}$]. Distributions for: **a**, mitigation pathways minus an “average” no mitigation pathway; **b**, mitigation pathways minus a “worst case” no mitigation pathway; **c**, mitigation and no mitigation pathways, minus the observed trend for the past 20 years (2000-2019; observational datasets used are those in Supplementary Fig. 1). Trends are calculated from FaIR projections plus an observation-based estimate of internal variability (see Methods). See the main text for details on how the distributions were calculated.

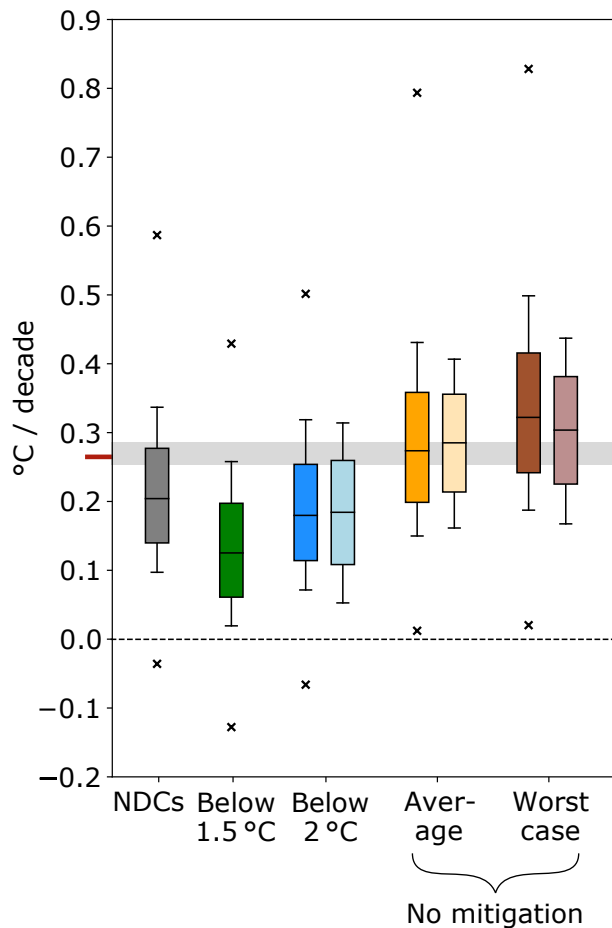
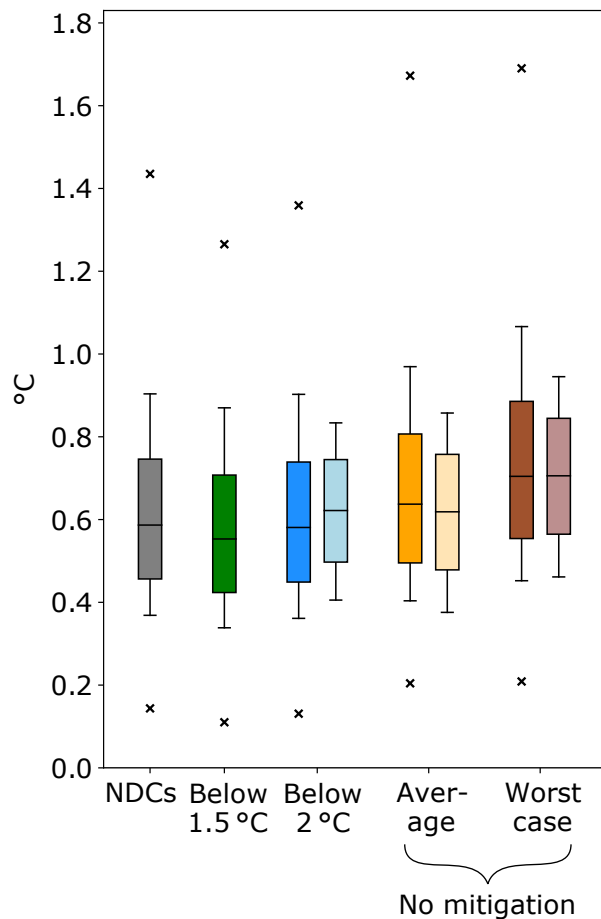
Figure 3: Global mean surface air temperature trends from FaIR starting in 2021, for different end years or trend lengths [$^{\circ}\text{C decade}^{-1}$]. Median trends are shown by colored solid lines, and the 17-83% (66% probability) range in trends is shown by colored shading. Trends are calculated from FaIR projections plus an observation-based estimate of internal variability (see Methods). Data are shown for emissions pathways consistent with: very strong mitigation in line with limiting warming to below $1.5\text{ }^{\circ}\text{C}$ (SSP1-1.9, green); strong mitigation in line with limiting warming to below $2\text{ }^{\circ}\text{C}$ (SSP1-2.6, blue); “average” no policy baseline scenario (SSP3-7.0, orange); and “worst case” no mitigation scenario (SSP5-8.5, brown). Black shading/line

shows the range/mean of maximum historical trends for different trend lengths from four different observation-based records (GISTEMPv4, CWv2 updated with HadSST3, HadCRUT4.6, and BE; see Supplementary Fig. 1). To compare with the model simulated GSAT projections, the observation data have been converted from GBST to GSAT using a scaling factor of 1.087 for BE, CWv2, and GISTEMPv4, and 1.19 for HadCRUT4.6 (see Methods). The gray vertical line highlights the year 2040, or a trend length of 20 years, which corresponds to the trend distributions for 2021-2040 shown in Fig. 1a.

Tables

Table 1: The probability of experiencing different near-term (2021-2040) global mean surface air temperature trends, as a result of following a mitigation pathway rather than a no mitigation pathway. a, The probability of the near-term temperature trend in a mitigation scenario ($\text{trend}_{\text{mit}}$) being lower than in a no mitigation scenario ($\text{trend}_{\text{nomit}}$) by a factor α ($P(\text{trend}_{\text{mit}} < \text{trend}_{\text{nomit}} - \alpha \times \text{trend}_{\text{nomit}})$). For $\alpha = 0$, the probabilities are calculated from the distributions in Fig. 2a and 2b; for $\alpha = 0.2$ and $\alpha = 0.4$, they are calculated by shifting the same distributions by amount $\alpha \times \text{trend}_{\text{nomit}}$. **b,** The probability, P_{ns} , that mitigation is both necessary and sufficient to experience a near-term temperature trend that is smaller than the trend observed, $\text{trend}_{\text{obs}}$, over the past 20 years (2000-2019). P_{ns} is given by $P_{\text{mit}} - P_{\text{nomit}}$, where $P_{\text{mit}} = P(\text{trend}_{\text{mit}} < \text{trend}_{\text{obs}})$ and $P_{\text{nomit}} = P(\text{trend}_{\text{nomit}} < \text{trend}_{\text{obs}})$. P_{mit} and P_{nomit} are calculated from the distributions in Fig. 2c. Probabilities are shown for mitigation pathways consistent with current and projected Nationally Determined Contributions (NDCs), very strong mitigation in line with limiting warming to below 1.5 °C (SSP1-1.9), and strong mitigation in line with limiting warming to below 2 °C (SSP1-2.6); and no mitigation pathways consistent with an “average” no policy baseline scenario (SSP3-7.0), and a “worst case” no mitigation scenario (SSP5-8.5).

Scenario comparison	a $P(\text{trend}_{\text{mit}} < \text{trend}_{\text{nomit}} - \alpha \times \text{trend}_{\text{nomit}})$			b $P_{\text{ns}} = P_{\text{mit}} - P_{\text{nomit}}$		
	$\alpha = 0$	$\alpha = 0.2$	$\alpha = 0.4$	P_{mit}	P_{nomit}	P_{ns}
Below 1.5 °C versus “average” no mitigation	0.91	0.83	0.67	0.88	0.25	0.63
Below 2 °C versus “average” no mitigation	0.80	0.65	0.43	0.69	0.25	0.43
NDCs versus “average” no mitigation	0.74	0.56	0.32	0.57	0.25	0.32
Below 1.5 °C versus “worst case” no mitigation	0.96	0.90	0.77	0.88	0.12	0.76
Below 2 °C versus “worst case” no mitigation	0.89	0.77	0.56	0.69	0.12	0.57
NDCs versus “worst case” no mitigation	0.85	0.70	0.46	0.57	0.12	0.46

a 2021-2040 GSAT trend**b** 2021-2040 GSAT anomaly

x max

95%

83%

median

17%

5%

x min

FaIR

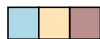
+ IV



CMIP6

with

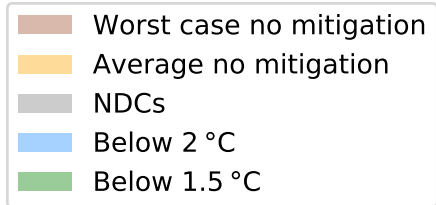
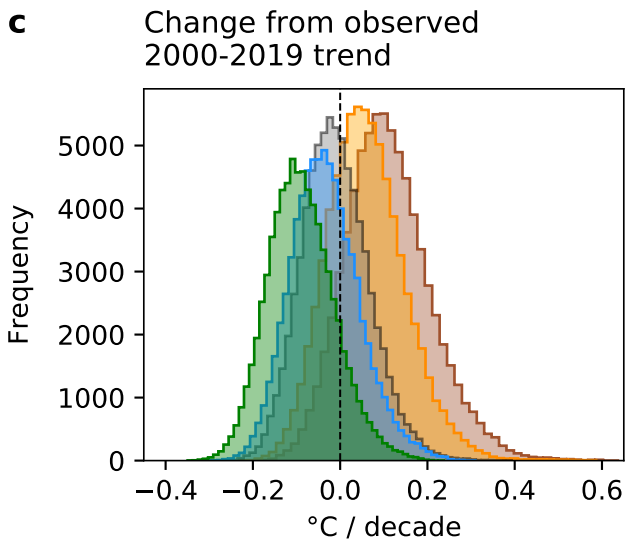
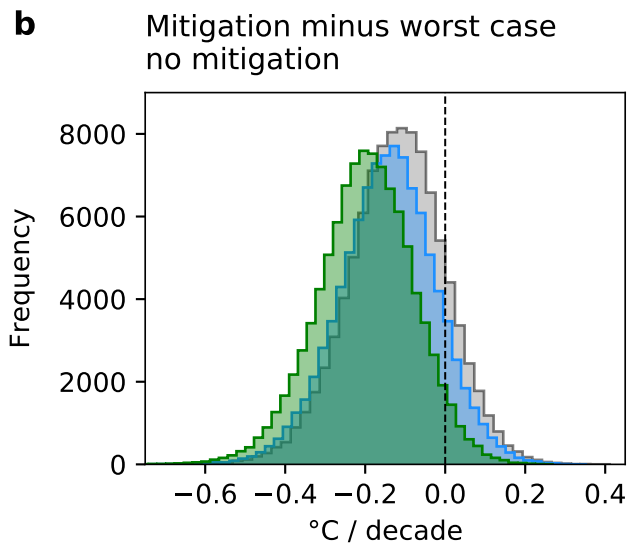
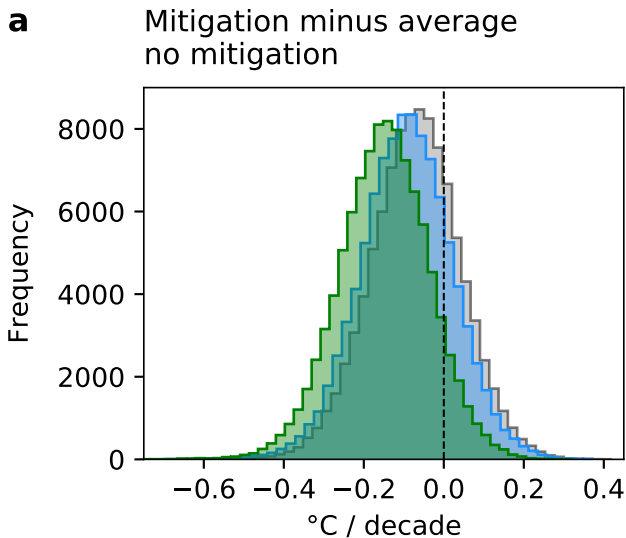
constraint



— mean

Max trend for
20-year segments
of observational
record

2021-2040 GSAT trend distributions from FaIR plus IV



GSAT trends from FaIR starting in 2021
for different end years or trend lengths

